Journal of the Korean Ceramic Society
Vol. 49, No. 4, pp. 385~396, 2012.

http://dx.doi.org/10.4191/kcers.2012.49.4.385

Review

Thermal Shock Tests and Thermal Shock Parameters for Ceramics

Hideo Awaji and Seong Min Choi*,†

King Mongkut's University of Technology Thonburi, Department Tool and Materials Engineering, Bangmod, Thongkru, Bangkok 10140, Thailand
**Fuji Electric Corporation of America, Edison, NJ 08837, USA*

(Received May 31, 2012; Revised July 5, 2012; Accepted July 10, 2012)

ABSTRACT

Thermal shock test methods and thermal shock parameters for ceramics were reviewed from the following viewpoints: (1) The test methods should be based on the precise estimation of both temperature and thermal stress distributions in a specimen taking into account the temperature-dependent thermo-mechanical properties; (2) The thermal shock parameters must be defined as a physical property of the materials and described as a function of temperature at the fracture point of the specimen; (3) The relation between the strength and fracture toughness of brittle ceramics under a thermal shock load must be the same as the relation under a mechanical load. In addition, appropriate thermal shock parameters should be defined by the thermal shock strength and thermal shock fracture toughness based on stress and energy criteria, respectively. A constant heat flux method is introduced as a testing technique suitable for estimating these thermal shock parameters directly from the electric power charged.

Key words : Thermal shock test, Thermal shock parameters, Brittle ceramics, Strength, Fracture toughness

1. Introduction

Due to their excellent heat resistance, structural ceramics are widely used in industrial fields that require the use of high temperature components. Ceramic crystals, however, have covalent and/or ionic bonds and tend to be brittle because dislocation movement is difficult. Therefore, ceramics are sensitive to the thermal stress associated with steep temperature gradients, i.e., thermal shocks. Thus, a precise evaluation of the thermal shock properties in ceramics is essential for them to be used reliably in high temperature structures.

Thermal shock fracture occurs with transient temperature variation over a short time range and the phenomenon of thermal shock fracture is normally rather complicated. In addition, thermo-mechanical properties of ceramics usually have strong temperature dependencies, which makes analysis of the temperature and stress distributions difficult, as mentioned by many researchers.[1-8] Therefore, it is essential to calculate the precise temperature and thermal stress distributions in a specimen and to measure the time-to-failure at the fracture point of the specimen during thermal shock testing. The thermal shock parameters should be estimated as a physical property of materials, measured directly from the thermal loading, and described as a function of temperature at the fracture point of the specimen. Several thermal shock parameters were proposed by Kingery[9] according to thermal environments and specimen configurations. Hasselman[10] developed the concept of thermal shock parameters and proposed a new thermal shock parameter called the thermal shock damage resistance.[11] Davidge and Tappin,[12] Awaji,[13] Lu and Fleck,[14] and Collin and Rowcliffe[15] suggested that thermal shock parameters should be based on two distinct failure criteria for brittle ceramics: a stress criterion where fracture occurs at the maximum tensile stress, and an energy criterion where a crack propagates when the stress intensity factor reaches the fracture toughness.

In this review, thermal shock test methods and thermal shock parameters for ceramics were surveyed by focusing on the following viewpoints: (1) The test method should be based on the precise estimation of both temperature and thermal stress distributions in a specimen, taking into account the temperature-dependent thermo-mechanical properties; (2) The thermal shock parameters must be defined as a physical property of the material and described as a function of temperature at the fracture point of the specimen; and (3) The relation between the strength and fracture toughness of brittle materials under a thermal shock load must be the same as the relation under a mechanical load when mild thermal shock tests are considered.

A standardized testing method for determining substantial thermal shock parameters can only be developed by selecting fundamental and relevant thermal shock parameters from the many that have been proposed to date. These parameters should represent the physical properties of the materials and be described as a function of temperature. Each material should be characterized by two parameters at the onset of

†Corresponding author : Seong Min Choi
E-mail : schoi@fecoa.fujielectric.com
Tel : +1-848-219-8469 Fax : +1-201-368-8258

fracture. One parameter must be the thermal shock strength, which represents the resistance of the material to fracture; the other parameter must be the thermal shock fracture toughness, which stands for the resistance of the materials to the onset of crack propagation.[13,16]

The discussion in this work is restricted to the uncoupled thermally induced stress problems; coupled and dynamic effects are not considered. Takeuchi and Furukawa[17] mentioned that these effects on the temperature and stress distributions in the materials are small when the Biot modulus is less than 10, where the Biot modulus is defined as $\beta = hl/\lambda$, (h: the heat transfer coefficient, l: the half-thickness of the plate, and λ: the thermal conductivity). In addition we will omit R-curve and fatigue failure behaviors under thermal shock loading in this review.

2. Thermal Shock Testing Methods

2.1. Cooling methods

Water quenching is widely used in the industry because of its simplicity. ASTM C1525-04 prescribes the determination of resistance to thermal shock in advanced ceramics by water quenching. This method is based on the idea of the Hasselman plot,[18] in which heated flexure specimens are quenched by a cold water bath. Subsequent flexure tests on the quenched specimens give the relation between strength degradation and temperature differential. The critical temperature differential is established from the temperature differential that produces a 30% reduction in flexural strength.

JIS R 1615 provides a procedure for quenching ceramics in water. It prescribes that the specimen configuration should be a pencil-shaped circular cylinder to avoid drag from atmospheric air in water, based on the research of Sakuma et al.[19] and that a statistical approach to crack appearance on the specimen surface should be used to estimate the critical temperature differential.[20] However, the critical problem in the water quenching is that water exhibits complicated boiling behavior on the specimen surfaces when the heated specimen is quenched in cold water. Becher et al.[1] mentioned the absence of quantitative agreement between thermal shock parameters and observations and explained that specimen geometry and size could be a factor in the thermal shock resistance because the Biot modulus is a function of the characteristic heat transfer length. The Biot modulus is also affected by specimen density,[21] drop height of the specimen,[22] and the bath and the specimen temperatures.[23] Furthermore, the critical temperature differential is not a physical property of materials[13] and not a reliable indicator of the onset of thermal shock fracture, as mentioned by Faber et al.[2] and Rogers and Emery.[24] Several alternative cooling media, including liquid metals,[25-27] salt,[28] air-jet,[2,5,29-32] oil,[33-36] helium gas,[37] a fluidized bed,[38] and water-jet[39] were used to minimize the effect of boiling on the heat transfer coefficient of the specimen and assure mild heat transfer conditions. Other cooling media included liquid nitrogen for superconducting materials, used by Osterstock et al.,[40] and a cooled brass rod that pressed on a specimen surface, as proposed by Rogers and Emery.[24]

Thermo-mechanical properties of ceramics normally have strong temperature dependencies, and the phenomenon of thermal shock fracture occurs with transient temperature variation over a short time range. Therefore, it is necessary to calculate precise temperature and thermal stress variations and estimate the temperature-at-failure and the time-to-failure. The time-to-failure in thermal shock experiments is detected by acoustic emission (AE) equipment. AE signals are very sensitive to crack propagation and the growth of micro- and macro-cracks.[8, 24,41]

To resolve the problems inherent in water quenching, Tanaka[42] proposed a novel technique called the water-flow cooling (WFC) technique, as shown in Fig. 1. The technique utilized a constant water-flow as a cooling medium to control the heat transfer coefficients on the cooling surface of the specimen. The WFC specimen covered with an insulator was constantly heated in an electric furnace while touching the cold water-flow, which cooled the specimen's surface. Accordingly, the heat transfer coefficient showed less fluctuation that conventional water quench tests. In this case, the Biot modulus was a small value at approximately 1. Furthermore, the complicated boiling phenomenon on the specimen surface was not present, and the relation between the heat transfer coefficients and the temperature of the specimen surface became almost constant. This observation was crucial because the thermal stress resistance is strongly influenced by the heat transfer coefficient observed in traditional water quench tests, as described by Becker.[43] In this technique, no edge or corner effects were observed on the specimen.[44] In addition, the fact that β is almost 1 is favorable for the thermal shock strength, R_{1C}, which will be explained in 3.1.

Fig. 2 compares the average heat transfer coefficients (a) in a conventional water quench test[45] and (b) in the WFC test.[42] The heat transfer coefficients are indicated by the open circles in (a), by the solid circles at a water velocity of 0.2 ms^{-1} in (b), and by the open triangles at a water velocity

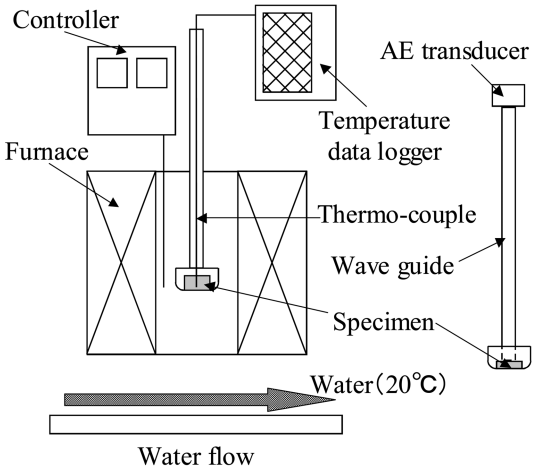

Fig. 1. Schematic diagram of the water-flow cooling test.

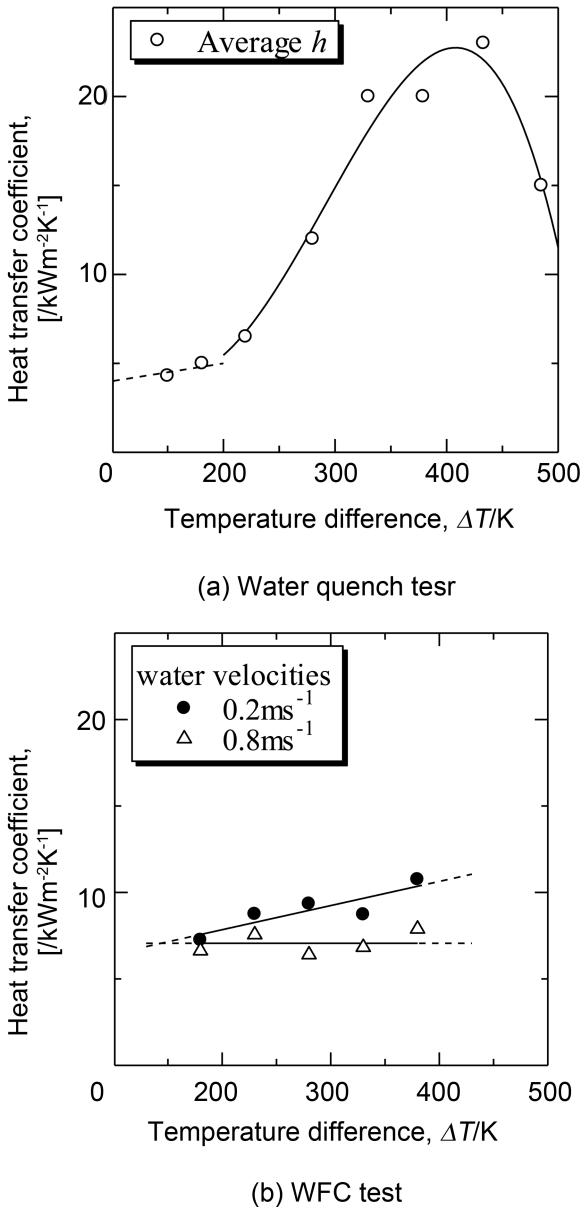

Fig. 2. Comparison of the heat transfer coefficients in (a) the water quench test and (b) the water-flow cooling test.

of 0.8 ms^{-1} in (b). In the water quench test, the average heat transfer coefficient varied from 5 to 23 [$kWm^{-2}K^{-1}$]. In the WFC test, the coefficients became almost constant when the velocity of the water was 0.8 ms^{-1}. The WFC technique was applied successfully for porous ceramics by Tanaka et al.[46] when the water-infiltrated in the pores of the material was taken into account.

2.2. Indentation method

After thermal shock testing, the retained strength for many specimens needed to be measured to estimate the critical temperature differential, ΔT_c. To reduce the number of specimens that needed to be measured, an indentation method was developed as an alternative approach.[2,15,33,47-54] A pre-crack with known geometry and position was used to remove many of the uncertainties in the specimen. Knoop indentation[2,47] and Vickers indentation[15,48-54] were used in water baths[15,47-52,54] or glycerin baths.[53]

However, Quinn and Bradt[55] described how the Vickers indentation test was not reliable in testing the fracture toughness of ceramics. One of the experimental problems for the Vickers indentation test was shown by Nawa et al.[56] in their study on TZP/Mo nanocomposites, where nanocomposites with more than 30 vol% Mo showed an abnormal increase in fracture toughness as measured by the IF (indentation fracture) method. Therefore, when using the Vickers indentation test, it is recommended to confirm the linear relation between $P^{2/3}$ and c in the behavior of the median-radial crack system in advance,[40] where P represents the indented load and c is the length of the radial crack.

2.3. Heating methods

Various heat sources could be used to evaluate the thermal shock resistance of brittle materials, such as arc-discharge or Joule heating,[57,58] moving electric beam,[59] laser beam,[60-63] hot gas-jet,[64] plasma jet,[65] electrical resistance heating,[4] and infrared radiation heating (IRH).[13,66,67] In the electrical resistance heating method, a ruthenium film was pasted on the peripheral surface of a circular disk specimen, and the assembly was heated by electrical resistance. The estimated effective heat flux was $(5\text{-}10) \times 10^5$ [$W \cdot m^2$] with laser beam heating, 4×10^7 [$W \cdot m^2$] with arc-discharge heating, and 1.5×10^5 [$W \cdot m^2$] with IRH.[68]

Benz et al.[60] proposed the parameter $\square \cdot t^{1/2}$ as a new measure to evaluate the thermal shock strength, where $\square$ and t represented the impinging energy flux of the laser and the pulse length, respectively. Akiyama et al.[61] and Amada et al.[62] used the critical power density of a laser as a measure of the thermal shock strength. Wei and Walsh[64] used the relation between the critical temperature differential and the probability of thermal shock failure to rank materials. Awaji and Sato[16] and Sato et al.[58] analyzed the stress intensity factor of a specimen shaped as a circular disk with an edge crack numerically and proposed the concept of thermal shock fracture toughness as a new thermal shock parameter, which will be explained in 3.2.

The arc-discharge heating method was developed by Sato et al.[57] to estimate the thermal shock strength of graphite, which has a high thermal shock resistance, using a specimen shaped as a circular disk. However, this technique was only applicable for electrically conductive materials. The IRH equipment was developed by Endo of Thermo-Riko Co. Ltd. in 1982,[69,70] which was used by Awaji to develop the IRH thermal shock test method for ceramics that was supported by Grants-in-Aid for Scientific Research from the Ministry of ESC Japan (1982 and 1984). The first paper on the IRH thermal shock test was published in 1995 by Awaji and Endo.[67]

Fig. 3 shows the schematics of the IRH equipment, where an IRH (halogen) lamp was placed at one focus of the ellipsoi-

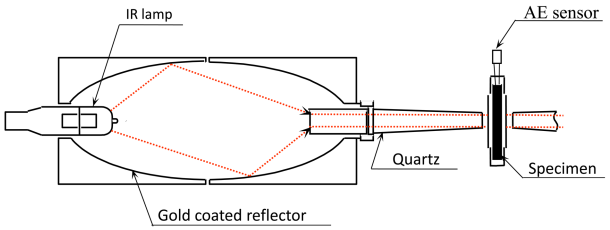

Fig. 3. Schematics of the infrared radiation heating equipment.

dal gold-coated reflector and the surface of the quartz rod was placed at the other focus. Two IRH sets were used to heat both sides of a circular specimen. The IRH technique was based on the concept of the arc-discharge heating method[57] and is applicable for materials that are not electrically conductive. The temperature and stress distributions were analyzed numerically taking into account the temperature-dependent thermo-mechanical properties using an implicit finite difference scheme based on the Crank-Nicolson method.[6,13,68] The thermal shock resistances to fracture and crack propagation were estimated in both the ambient and elevated temperature environments. Some experimental results are introduced in 3.3.

3. Thermal Shock Parameters

3.1. Problems of thermal shock parameters

To establish the thermal shock parameters as a physical property of the materials, the parameters should only be defined by fundamental and relevant parameters already proposed. Each material under thermal shock loading should be characterized by two parameters at the onset of brittle fracture[12-15]: thermal shock strength and thermal shock fracture toughness.[68] A rapidly cooled hot plate was used to illustrate a typical thermal shock environment and the associated problem of thermal stress: the environment was also used to introduce suitable thermal shock parameters. The relation between the temperature differential and the maximum thermal stress due to the cooling plate is expressed by the following well-known approximations[71]:

For a small Biot modulus,

$$\Delta T = \frac{\lambda \sigma_{max}}{E\alpha}\frac{3.25(1-\nu)}{hl}, \tag{1}$$

and for a large Biot modulus

$$\Delta T = \frac{\sigma_{max}(1-\nu)}{E\alpha}, \tag{2}$$

where ΔT represents the temperature differential, σ_{max} is the maximum thermal stress, E is Young's modulus, α is the thermal expansion coefficient, and ν is Poisson's ratio. Using the Biot modulus β and the normalized maximum stress defined as

$$\sigma^{*}_{max} = \frac{\sigma_{max}(1-\nu)}{E\alpha\Delta T}, \tag{3}$$

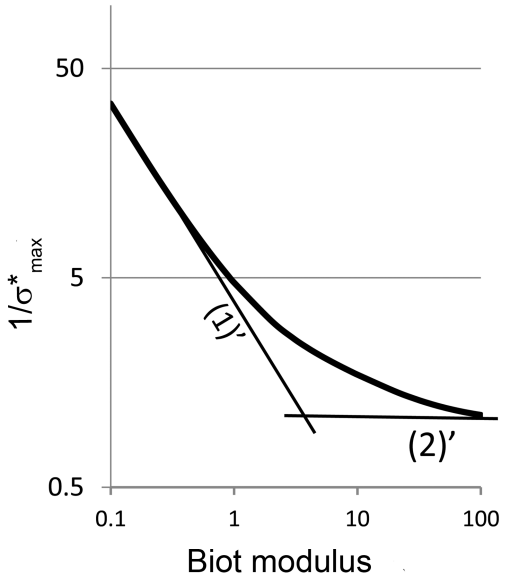

Fig. 4. Relation between the Biot modulus and the normalized maximum thermal stress in a cooled plate, where the solid curve represents the exact relation and the two straight lines indicate Eqs. (1)' and (2)'.

Eqs. (1) and (2) could be rewritten as

$$\frac{1}{\sigma^{*}_{max}} = \frac{3.25}{\beta}, \tag{1}'$$

and

$$\sigma^{*}_{max} = 1. \tag{2}'$$

Fig. 4 shows the exact relation between the normalized maximum thermal stress and the Biot modulus indicated by the bold curve; the approximations by Eqs. (1)' and (2)' are indicated by the two thin solid lines. As seen from Fig. 4, Eq. (1)' gave a better approximation in the range of β □ 1, and Eq. (2)' was only applicable in the range of $\beta > 100$.

Eliminating the numerical constant and the factors related to the thermal and experimental environment from the right-hand side of Eq. (1), i.e., 3.25, h (cooling condition), l (specimen configuration), and (1-ν) (biaxial stress state), the critical value of the combination of the material properties is expressed for a mild thermal shock test as[13,68]

$$R_{1C} = \frac{\lambda \sigma_B}{E\alpha}, \tag{4}$$

where R_{1C} represents the thermal shock strength under the critical temperature differential ΔT_C and σ_B is the strength of the material. The thermal shock strength characterizes the resistance of a material to the onset of fracture and is, therefore, one of the physical properties of the material.

The classical thermal stress resistance parameters are expressed as[11,72]

$$R = \frac{\lambda \sigma_B (1-\nu)}{E\alpha} \quad \text{for a small Biot modulus,} \tag{5}$$

and

Table 1. Comparison between the Static Fracture of a 3-point Flexure Specimen and the Thermal Shock Fracture in a Cooled Plate

	Static fracture	Thermal Shock Fracture
Load	P	ΔT
Stress	$\sigma_{max} = P/D \propto P$	$R_1 = \lambda\sigma_{max}E\alpha\propto\Delta T$
Strength	$\sigma_c = P_c/D \propto P_c$	$R_{1c} = \lambda\sigma_{max}E\alpha\propto\Delta T_c$
Stress Intensity Factor	$K_I=P/DY(n)H^{1/2}\propto P_c$	$R_2 = \lambda K_I E\alpha\propto\Delta T_c$
Fracture Toughness	$K_{IC}=P_c/DY(n)H^{1/2}\propto P_c$	$R_{2c} = \lambda K_{IC}E\alpha\propto\Delta T_c$

P = flexure load; D = 2BH^2/3S; B, width; H, height; S, span length; $n = c/H$; c, edge crack depth; Y, shape factor

$$R=\frac{\sigma_B(1-\nu)}{E\alpha} \text{ for a large Biot modulus.} \quad (6)$$

As mentioned previously, the term $(1-\nu)$ in these equations should be eliminated. Many researchers referenced Eqs. (5) and (6), but Mai and Atkins,[73] Lewis,[74] Anzai and Hashimoto,[75] and Rogers and Emery[24] stated that no agreement existed between the thermal shock resistance parameter and the critical temperature differential, ΔT_C. Furthermore ΔT_C is not a reliable indicator of the onset of thermal shock fracture, as Table 1 illustrates.

For a plate with a crack under mode I loading, the stress intensity factor is given in the following general form as

$$K_1=B\sigma_\theta\sqrt{\pi c}\,, \quad (7)$$

where B represents the shape factor, σ_θ is the normal stress, and c is the half-crack length. By substituting Eq. (7) into Eq. (1), the following equation is derived:

$$\Delta T=\frac{\lambda K_I}{E\alpha}\frac{3.25(1-\nu)}{hlB\sqrt{\pi c}}\,. \quad (8)$$

Eliminating the factors related to the thermal and experimental environments from the right-hand side of Eq. (8), the critical value of the combination of the material properties is expressed for a mild thermal shock test as[13,68]

$$R_{2C}=\frac{\lambda K_{IC}}{E\alpha}\,, \quad (9)$$

where R_{2C} represents the thermal shock fracture toughness,[58] and K_{IC} represents the intrinsic fracture toughness of the materials. The thermal shock fracture toughness represents the resistance of a material to the onset of crack propagation under thermal shock loading and is one of the physical properties of the materials.

Table 1 explains the analogy between the static fracture by a three-point flexure test and the thermal shock fracture in a cooled plate. In this table, P represents the flexure load, P_c is the critical load, $D = 2BH^2/3S$, B and H is the width and height of the flexure specimen, respectively, S is the span length, Y is the shape factor, $n = c/H$, and c is the length of the edge crack. The temperature differential ΔT under thermal shock corresponds to the load P under a static load. Furthermore, the critical values ΔT_c and P_c are not material constants[24] because they contain factors related to thermal and experimental environments. Only the strength factors (σ_C and R_{IC}) and the fracture toughness factors (K_{IC} and R_{2C}) could be treated as material constants.

3.2. A constant heat flux method

The usefulness of the thermal shock parameters R_{1C} and R_{2C}, mentioned above could be limited if they could not be evaluated directly from thermal loading like the conventional parameters. However, the constant heat flux method made it possible to evaluate these parameters directly from the electric power charged. The heat flux q into the circular disk specimen is calculated from the electric power for the arc-discharge heating method and the IRH method as

$$q=\frac{\eta W}{\pi a^2}\,, \quad (10)$$

where η represents the efficiency of the heat flux, W is the electric power, and a is the radius of the heating area.

The transient thermal stress in a circular disk was analyzed based on the temperature distribution using Timoshenko and Goodier's well-known quasi-static analytical method[76]. The maximum value of the circumferential stress increased with an increase in the normalized heating time, τ, defined as

$$\tau=\frac{\kappa t}{R^2} \quad (11)$$

where κ represents the thermal diffusivity, t is the actual heating time, and R is the radius of the disk. The normalized maximum stress S_{max} is defined as

$$S_{max}=\frac{\sigma_{\theta max}}{E\alpha Q}\,, \quad (12)$$

where $\sigma_{\theta max}$ represents the maximum circumferential stres, $Q = qR^2/\lambda H$, and H is the thickness of the disk. Therefore, the thermal shock strength could be expressed in terms of the electric power charged, W, and the maximum thermal stressat the fracture point, S_c, using Eqs. (4), (10), (12), and Q as

$$R_{1C}=S_c\frac{\eta W}{\pi H(\alpha/R)^2}\,. \quad (13)$$

The thermal shock strength could then be estimated directly from W and S_c at the fracture point.

In the same manner, the thermal shock fracture toughness could be estimated using a circular disk with an edge crack.[16,58,68] The normalized stress intensity factor N_I is

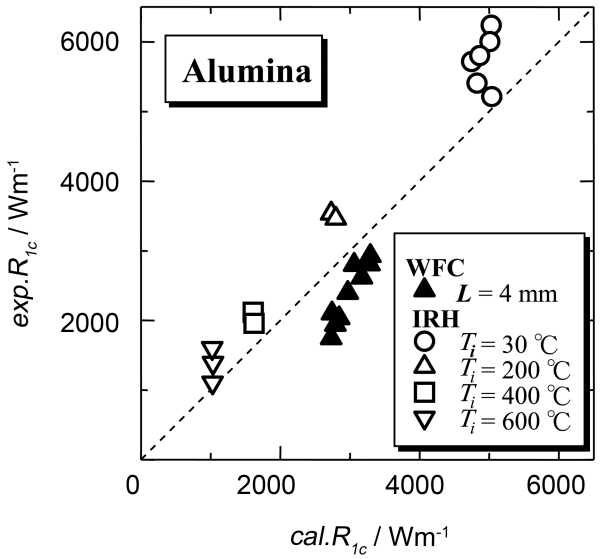

Fig. 5. Relation between the experimentally obtained R_{IC} ($exp.R_{1C}$) and calculated R_{1C} ($cal.R_{1C}$). The infrared radiation heating results are shown by open symbol marks, and the water-flow cooling results are shown by solid triangles.

defined as

$$K_1 = N_1\sqrt{\pi c}E\alpha Q\,. \tag{14}$$

where c indicates the depth of the edge crack. Then, the thermal shock fracture toughness is expressed as

$$R_{2c} = N_{IC}\sqrt{\pi c}\frac{\eta W}{\pi H(a/R)^2}\,. \tag{15}$$

The thermal shock fracture toughness could be determined by the electric power, W, and the normalized critical stress intensity factor, N_{IC}, as the crack begins to propagate. The thermal shock test with a constant heat flux thus provided a direct 'en bloc' measurement of both the thermal shock strength and the thermal shock fracture toughness from the electric power charged.[58]

3.3. Experimental results

Some experimental results of the WFC and IRH tests were introduced briefly in.[78] Only the thermal shock strength was considered in this study. The stress distribution and size effects on the fracture strength between the flexure specimen and the circular disk specimen used for the thermal shock study were modified using Weibull statistics. Commercially available alumina was used for the tests. In Fig. 5, the vertical axis indicates the experimentally obtained R_{1C}, noted as $exp.R_{1C}$, and the horizontal axis is the calculated values of the combination of the fracture strength σ_B and other temperature-dependent material properties such as λ, E, and α that are shown in Eq. (4). This calculated value is noted as $cal.R_{1C}$. The open marks ○, △, □, and ▽ represent the results of the IRH test,[78] and the solid triangles are the results of the WFC test.[42] A relatively good correlation was observed between the $exp.\ R_{IC}$ and the $cal.\ R_{IC}$, and the R_{1C} in the IRH test decreased as the initial temperatures T_i for the preheated specimens increased from 30 to 600°C. At around room temperature, the R_{1C} had the highest value among the data. As a consequence, the R_{1C} is recognized as the temperature-dependent material property.

4. Related Topics

4.1. Measurement of heat transfer coefficients

Whereas the temperature and thermal stress distributions are strongly influenced by the heat transfer coefficient h, the h value depends on factors such as ΔT, the turbulence of the medium, the incidence of boiling, and the shape of the body[1,2,21-23,79]. The h value in a water quench test varies significantly during a short time range, and experimentally obtained results are limited. Singh et al.[23] inferred the h value versus film temperature from the experimental ΔT_c values during a water quench test. Rogers et al.[79] calibrated the h value based on the probability of failure. Sakuma et al.[80] estimated the h values for water, silicone oil, and liquid sodium baths using a pencil-shaped silver (λ = 429 $Wm^{-1}K^{-1}$) specimen. Lee et al.[81] measured the h value of ceramic specimens using a thin-foil of a "cement-on" K-type thermocouple. Nishikawa et al.[82] measured the transient temperature to estimate the h value using a thermocouple and a double-thermocouple technique in a zirconia specimen that has a small temperature-dependent thermal conductivity. Tomba and Cavalieri[30] estimated the h value by fitting calculated temperature profiles with measured temperatures during the air jet cooling test. Honda et al.[45] used a pencil-shaped nickel (λ = 90.9 $Wm^{-1}K^{-1}$) specimen for a water quench test, shown in Fig. 2(a). Tanaka et al.[42] used a silver plate specimen for the WFC tests, shown in Fig. 2(b).

4.2. Temperature/stress analyses and damage detection

To estimate thermal shock parameters, the temperature and stress distributions in a thermal-shocked specimen need to be precisely calculated taking into account the temperature-dependent thermo-mechanical properties. Even though Mizutani et al.[4] used an imperfect one-dimensional heat conduction equation, they applied a variable transformation technique to the finite difference method to analyze the non-linear heat conduction equation with temperature-dependent thermal properties. Tanaka et al.[42] and Awaji et al.[6] analyzed one-dimensional and axi-symmetric non-linear heat conduction equations using an implicit finite difference method based on the Crank-Nicolson scheme, where the thermo-mechanical properties were approximated by polynomial equations of temperature, and applied the variable transformation technique. Mignard et al.[5] analyzed a two-dimensional heat conduction equation with temperature-dependent thermal properties while using finite differences and finite elements to solve the non-linear heat conduction equations. Several researchers used finite element methods

to analyze temperature and stress distributions taking into account the temperature-dependent thermo-mechanical properties.[2,7,24,29,30] In a water quench test, some crack on a specimen could be extended by stress corrosion cracking (SCC).[8,79,83] Badaliance et al.[83] showed the significance of SCC on the thermal stress resistance of a material. Rogers et al.[79] mentioned that two distinct flaw populations were present in a water quenched specimen: the initial flaws and the extended cracks due to thermal shock. Awaji et al.[84] measured the retained strength of water quenched alumina and observed three statistical distributions: the initial inert strength, the retained strength of the thermally shocked specimen without thermal shock cracking, and the retained strength with thermal shock cracking. The thermally shocked specimens contained more or less SCC behavior. The critical temperature differential was statistically estimated using the original distributions of the retained strength without thermal shock cracks.

Nondestructive techniques were proposed by several researchers to estimate the relation between thermal shock temperature and damage.[5,7,29,85-90] Oguma and Motomiya[85] proposed the BET (Brunauer-Emmett-Teller) method to detect surface crack areas. This method could detect the critical temperature differential, but it could not detect interior cracks. Hefetz and Rokhlin,[86] Vedula et al.,[29] and Boccaccini et al.[87] used an ultrasonic technique to estimate damage. Lee and Case[88] employed non-destructive measures to determine the elastic modulus and internal friction. Mignard et al.[5,89,90] used an AE technique to obtain the direct relation between AE and thermal shock degradation.

4.3. Thermal shock tests for special materials

Vandeperre et al.[91] studied the influence of crack-deflection at the interlayer of the layered material on the thermal shock behavior of the material. Sherman[92] constructed an alumina/metal laminate by alternating alumina plates and nickel/copper foils and conducted a water quench test. The design of functionally graded materials (FGMs) is now focused on optimizing the material structure to yield appropriate residual stresses and minimizing the thermal stresses under thermal shock loading. Kokini et al.[93] tested functionally graded thermal barrier coating. Kawasaki and Watanabe[94] evaluated the thermal fracture behavior of metal/ceramic FGMs by heating them with a burner. Wang et al.[95] introduced a finite element/finite difference method to analyze the time-dependent temperature distributions in a material by taking into account the temperature-dependent material properties. Jin et al.[96,97] fabricated mullite/Mo FGM plates using a powder metallurgy process and estimated the thermal shock properties by combining the IRH and WFC techniques.

5. Strength and Fracture Toughness

5.1. Strength of ceramics

Microstructural-level residual stresses occur in polycrystalline ceramics during the cooling process after sintering due to anisotropic thermal expansion and crystallographic misorientation across the grain boundaries[98]. Gupta[99] reported that the internal residual stresses caused by the thermal expansion anisotropy were observed in polycrystalline alumina and showed that the material with larger grain size had lower strength. The magnitude of these stresses was sufficiently high according to the grain size. Evans[100] analyzed residual stresses caused by thermal expansion anisotropy in polycrystalline ceramics and clarified that stress was intensified the most at the triple point of the grain boundary. Vedula et al.[98] and Zimmermann et al.[101] simulated the residual stress in polycrystalline alumina using a finite element code.

It should be noted that sintered polycrystalline ceramics typically have large amount of residual stresses in the grains, and the residual stresses are in a self-equilibrium state in the specimen. If a certain grain has a tensile residual stress, the neighboring grains would have compressive stresses.[102] Thus, it is conceivable that the strength of the specimen would significantly decrease if tensile residual stresses were present around the weakest defect. Nanocomposites proposed by Niihara[103] had special strengthening mechanisms explained by the residual stress release mechanism[102,104]. An example is shown in Fig. 7 and Table 2, which will be explained later. The fracture toughness of ceramics, however, is rarely affected by the residual stresses as long as the fracture toughness is measured with large pre-cracks. In addition, the strength of brittle materials depends strongly on the size of the weakest defect inherent in the material, and the experimentally obtained strength of ceramics depends on the specimen volume under tensile and shear stresses and the stress state. Hence the strength of brittle materials needs to be treated statistically and not as a physical property, whereas fracture toughness is a more well-defined physical property.[15] To discuss the relation between the material strength and fracture toughness, a new concept of intrinsic strength with no size effect needs to be defined.

5.2. Intrinsic strength

The intrinsic strength of ceramics is estimated as follows.[102] Consider a crack in an infinite plate of brittle ceramics under mode I loading. The exact normal stress σ_y on the r-axis, as shown in Fig. 6, is analyzed by Okamura[105] as

$$\sigma_y = \frac{\sigma_f(a_e + r)}{\sqrt{2a_e r + r^2}}, \tag{16}$$

where σ_f represents the remote stress on the plate, a_e is the half-crack length, and r is the distance from the crack tip. Although the J-integral based on non-linear elastic fracture analysis is applicable widely, a fracture criterion for brittle ceramics is usually expressed by the linear elastic fracture mechanics (LEFM). Assuming that the crack length in the specimen is sufficiently long compared with the frontal process zone (FPZ) size, the Griffith-Irwin criterion for the crack extension based on the LEFM can be

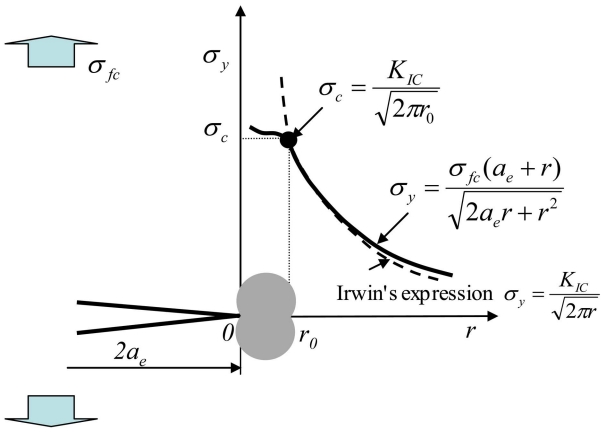

Fig. 6. Stress distribution ahead of a crack tip in an infinite plate with a long crack.

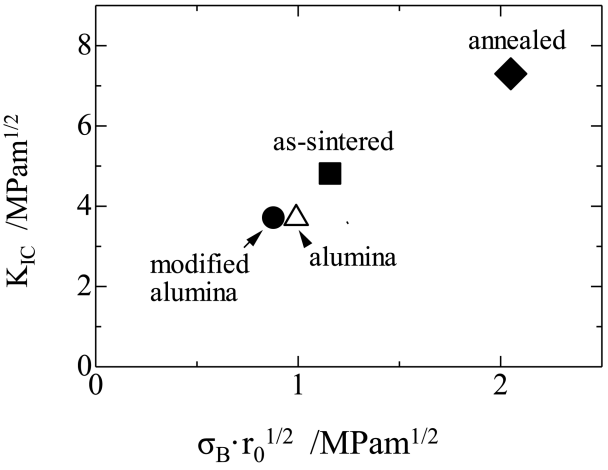

Fig. 7. Relation between fracture toughness and $\sigma_B r_0^{1/2}$.

expressed as,

$$\frac{K_{IC}^2}{E'} = 2\gamma_I, \tag{17}$$

where $E' = E$ for the plane stress state, $E' = E/(1-\nu^2)$ for the plane strain state, and γ_I is the fracture energy per unit crack extension consumed in the FPZ formation. Fig. 6 shows the relation between the exact stress distribution on the r-axis expressed by Eq. (16) and Irwin's K-value approximation for the case of a long crack under a critical stress state. In this case, the crack length is sufficiently long compared with the FPZ size r_0, σ_{fc} represents the critical remote stress on the plate, and σ_c is the critical local stress on r_0 based on the local fracture approach. Then, the normal stress distribution σ_y can be approximated using Irwin's expression in the vicinity of r_0 as ,

$$\sigma_y = \frac{K_{IC}}{\sqrt{2\pi r}}, \tag{18}$$

and the relation between the critical local stress σ_c at r_0 is expressed as

$$\sigma_c = \frac{K_{IC}}{\sqrt{2\pi r}} \tag{19}$$

Equation (19) implies that K_{IC}, r_0, and σ_c are mutually dependent material constants and the σ_c value can be calculated from the values of K_{IC} and r_0. In addition, the global approach of the Griffith-Irwin criterion and the local approach of the local fracture criterion become identical at r_0 in the case of a long crack.

On the other hand, the LEFM is not normally applicable to the inherent flaws in ceramic materials.[102,104] For such a short crack problem, Eq. (16) must be used to calculate the critical local stress. In this case, the stress at r_0 under a critical stress state is expressed as

$$\sigma_c = \frac{\sigma_{fc}(a_e + r_0)}{\sqrt{2a_e r_0 + r_0^2}}. \tag{20}$$

The strength σ_{fc} of the infinite plate with the half-crack length a_e is hence given by

$$\sigma_{fc} = \sigma_c \frac{\sqrt{2a_e r_0 + r_0^2}}{a_e + r_0}. \tag{21}$$

Taking the limit a_e to zero in Eq. (21), the following relation is derived:

$$\lim_{a_e \to 0} \sigma_{fc} \to \sigma_c \tag{22}$$

Equation (22) indicates that σ_c has two significant meanings: the critical local stress ahead of a crack tip and the strength of an infinite plate with no crack. Therefore, σ_c is the inherent strength with no size effect and should be one of the fundamental properties of the material. The experimentally obtained relation between the flexure strength and the intrinsic strength was expressed in ref. 102.

5.3. Relation between strength and toughness

The critical FPZ size can be derived using a statistical treatment. Because the technique for estimating the critical FPZ size was expressed in ref. 102, only a summary is presented here. Equation (19) and the following formula were used to estimate the critical local stress,

$$\frac{\sigma_c}{\sigma_B} \approx \left\{ \frac{V_B}{V_{FPZ}} \right\}^{1/m}. \tag{23}$$

where V_B and V_{FPZ} represent the effective volumes of the specimen and the critical FPZ of ceramics, respectively, and m is a shape parameter of Weibull distribution. From Eqs. (19) and (23), the following relation between the strength and fracture toughness is derived under the small scale yielding condition:

$$K_{IC} = \sigma_c \sqrt{2\pi r_0} \propto \sigma_c \times r_0^{1/2} \propto \sigma_B \times r_0^{1/2}. \tag{24}$$

The equation describes the relation between the fracture toughness, the intrinsic strength, the critical FPZ size, and the flexure strength of brittle materials. The fracture strength is essentially proportional to the fracture toughness of brittle materials.

Table 2. Fracture Toughness, Flexure Strength, and Critical Frontal Process Zone Size for Alumina, As-sintered Alumina/Ni Nanocomposites, and Annealed Nanocomposites. The Flexure Strength of Alumina is the Measured Value and the Flexure Strength of Modified Alumina is the Modified Value Assuming the Strength Reduction by Residual Stress is 260 MPa.

	K_{IC} /MPam$^{1/2}$	σ_B /MPa	r_0 /μm
alumina	3.7	510	3.8
modified alumina	-	510+260	1/3
as-sintered nanocomposites	4.8	920	1.6
annealed nanocomposites	7.3	880	5.4

The sizes of the 3-point flexure specimen are B = 2.0, H = 2.0, S = 8.0 /mm.The Weibull shape factor is m = 16.

Hasselman's thermal shock damage resistance parameter[11] is modified under the plane strain condition as

$$R'''' = \left(\frac{K_{IC}}{\sigma_B}\right)^2 (1+\nu) . \quad (25)$$

After inserting Eq. (24) into Eq. (25), the R'''' parameter was seen to be proportional to r_0. Mai and Atkins[73] used the ratio $(K_{IC}/\sigma_B)^2$ to explain the retained strength of thermal-shocked specimens and showed that the retained strength of materials with a higher $(K_{IC}/\sigma_B)^2$ value could be improved significantly. It is known that materials with a larger critical FPZ size have higher fracture toughness, but there is no factor to express the thermal shock characters in Eq. (25). Hence the R'''' parameter is not an appropriate measure of the thermal shock resistance to crack propagation.

Fig. 7 shows the relation between K_{IC} and $\sigma_B \cdot r_0^{1/2}$ in monolithic alumina, as-sintered alumina-nickel nanocomposites, and annealed nanocomposites in an alumina-nickel (3 vol%) system.[106] A nearly linear relation was observed between K_{IC} and $\sigma_B \cdot r_0^{1/2}$. The experimentally obtained values of fracture toughness, flexure strength, and critical FPZ size are shown in Table 2, where the data are listed for monolithic alumina, modified alumina (the modification was performed assuming that the decrease of the strength due to residual stress was 260 MPa in this case), as-sintered alumina/3 vol% Ni nanocomposites, and annealed nanocomposites. The details were described in refs. 102 and 104. It is commonly known that the strength and fracture toughness of ceramics cannot always be simultaneously increased; typically, ceramics with higher strengths are more brittle and the materials with more stable crack propagation exhibit a lower strength.[15] However, in the case of Niihara's nanocomposites,[103] no tradeoff relation was observed between the strength and fracture toughness. In Eq. (24), it should be noted that K_{IC} represents the value of the inherent fracture toughness (the initial fracture toughness with no bridging on the crack surfaces), and the toughening mechanism based on crack-surface bridging cannot improve the inherent fracture toughness.[106] When the toughening mechanism of ceramics is based on the FPZ expansion mechanism as in the case of the alumina-nickel nanocomposites, both the fracture toughness and the strength are simultaneously improved.

The relation for the thermal shock parameters could be derived in the same manner as Eq. (24):

$$R_{2C} \propto R_{1C} \propto r_0^{1/2} . \quad (26)$$

This equation gives the proper relation between the thermal shock strength and thermal shock fracture toughness.

6. Conclusions

Methods to test thermal shock were reviewed based on the following viewpoints: the precise estimation of temperature and stress distributions, appropriate thermal shock parameters, and the relation between the strength and fracture toughness. The water-flow cooling method improved upon the conventional water quench cooling technique. Constant heat flux methods, such as the arc-discharge heating test, the Joule heating test, and the infrared radiation heating test, estimated the thermal shock strength and thermal shock fracture toughness directly from the electric power charged.

The thermal shock strength and thermal shock fracture toughness were defined as the physical properties of thermal shock resistance based on a stress criterion and an energy criterion. These thermal shock parameters were described as a function of temperature at the fracture point of the specimen. The relation between the thermal shock strength and the thermal shock fracture toughness was derived by comparing the strength and the fracture toughness under static mechanical loading.

REFERENCES

1. P. F. Becher, D. Lewis, K. R. Carman, and A. C. Gonzalez, "Thermal Shock Resistance of Ceramics: Size and Geometry Effects in Quench Tests," *Ceram. Bull.*, **59** [5] 542-45 (1980).
2. K. T. Faber, M. D. Huang, and A. G. Evans, "Quantitative Studies of Thermal Shock in Ceramics Based on a Novel Test Technique," *J. Am. Ceram. Soc.*, **64** [5] 296-301 (1981).
3. D. Lewis, "Thermal Shock and Thermal Shock Fatigue Testing of Ceramics with the Water Quench Test," Fracture Mechanics of Ceramics, Vol. 5, pp. 487-96, ed. R. Bradt, A. G. Evans, D. P. H. Hasselman, and F. F. Lange, 1983.
4. Y. Mizutani, T. Nishikawa, T. Fukui, and M. Takatsu, "Thermal Shock Fracture of Ceramic Disk under Rapid Heating," *J. Ceram. Soc. Jpn*, **103** [5] 525-28 (1995).

5. F. Mignard, C. Olagnon, G. Fantozzi, P. Chantrenne, and M. Raynaud, "Thermal Shock behavior of a Coarse Grain Porous Alumina," *J. Mater. Sci.*, **31** 2131-38 (1996).
6. H. Awaji, T. Takahashi, N. Yamamoto, and T. Nishikawa, "Analysis of Temperature/Stress Distributions in Thermal Shocked Ceramic Disks in Relation to Temperature-Dependent Properties," *J. Ceram. Soc., Jpn*, **106** [4] 358-62 (1998).
7. M. Hamidouche, N. Bouaouadja, C. Olagnon, and G. Fantozzi, "Thermal Shock Behavior of Mullite Ceramic," *Ceramics Int.*, **29** 599-09 (2003).
8. A. G. Evans, M. Linzer, H. Johnson, D. P. H. Hasselman, and M. E. Kipp, "Thermal Fracture Studies in Ceramic Systems Using an Acoustic Emission Technique," *J. Mater. Sci.*, **10** 1608-15 (1975).
9. W. D. Kingery, "Factors Affecting Thermal Stress Resistance of Ceramic Materials," *J. Am. Ceram. Soc.*, **38** [1] 3-15 (1955).
10. D. P. H. Hasselman, "Figures-of-merit for the Thermal Stress Resistance of High-temperature Brittle Materials: a Review," *Ceramurgia Int.*, **4** [4] 147-50 (1978).
11. D. P. H. Hasselman, "Unified Theory of Thermal Shock Fracture Initiation and Crack Propagation in Brittle Ceramics," *J. Am. Ceram. Soc.*, **52** [11] 600-04 (1969).
12. R. W. Davidge and G. Tappin, "Thermal Shock and Fracture in Ceramics," *Trans. British Ceram. Soc.*, **66** 405-22 (1967).
13. H. Awaji, "Thermal Shock Fracture Toughness by Infrared Radiation Heating Technique(*in Jpn*)," *Trans. JSME*, **62A** [595] 700-06 (1996).
14. T. J. Lu and N. A. Fleck, "The Thermal Shock Resistance of Solids," *Acta Mater.*, **46** [13] 4755-68 (1998).
15. M. Collin and D. Rowcliffe, "Analysis and Prediction of Thermal Shock in Brittle Materials," *Acta Mater.*, **48** 1655-65 (2000).
16. H. Awaji and S. Sato, "Stress Intensity Factor of an Edge Crack in a Disk and Thermal Shock Fracture Toughness *(in Jpn),*" *Jpn. Soc. Str. & Fract. Mater.*, **13** 78-85 (1978).
17. Y. Takeuchi and T. Furukawa, "Some Considerations on Thermal Shock Problems in a Plate," *J. Appl. Mech.,* **48** [3] 113-18 (1981).
18. D. P. H. Hasselman, "Strength Behavior of Polycrystalline Alumina Subjected to Thermal Shock," *J. Am. Ceram. Soc.*, **53** [9] 490-95 (1970).
19. T. Sakuma, U. Iwata, and H. Takaku, "Thermal Shock Resistance of Ceramics: A Novel Quenching Method and Non-Steady Heat Transfer Coefficients," in Experimental Heat Transfer, Fluid Mechanics, and Thermodynamics, pp. 537-44, Edited by J. F. Keffer, et al., Elsevier Science Pub. Co. ltd., 1991.
20. T. Sakuma, U. Iwata, H. Takaku, and N. Okabe, "Estimation of Thermal Shock Resistance of Ceramics (*in Jpn*)," *Trans. JSME*, **59A** 131-36 (1993).
21. J. P. Singh, J. R. Thomas, and D. P. H. Hasselman, "Analysis of Effect of Heat-Transfer Variables on Thermal Stress Resistance of Brittle Ceramics Measured by Quenching Experiments," *J. Am. Ceram. Soc.*, **63** [3-4] 140-44 (1980).
22. J. P. Singh, D. P. H. Hasselman, and G. Ziegler, "Effect of Drop Height on Critical Temperature Difference (ΔT_c) for Brittle Ceramics Subjected to Thermal Shock by Quenching into Water," *J. Am. Ceram. Soc.*, **66** [10] C194-95 (1983).
23. J. P. Singh, Y. Tree, and D. P. H. Hasselman, "Effect of Bath and Specimen Temperature on the Thermal Stress Resistance of Brittle Ceramics Subjected to Thermal Quenching," *J. Mater. Sci.*, **16** 2109-18 (1981).
24. W. P. Rogers and A. F. Emery, "Contact thermal Shock Test of Ceramics," *J. Mater. Sci.*, **27** 146-52 (1992).
25. J. Jung, A. Reck, and R. Ziegler, "The Compatibility of Alumina Ceramics with Liquid Sodium," *J. Nuclear Mater.,* **119** 339-50 (1983).
26. W. Dienst, H. Scholz, and H. Zimmermann, "Thermal Shock Resistance of Ceramic Materials in Melt Immersion Tests," *J. Eur. Ceram. Soc.*, **5** 365-70 (1989).
27. T. Sakuma, U. Iwata, and H. Takaku, "Estimation of Thermal Shock Resistance of Ceramics (*in Jpn*)," *Trans. JSME*, **58A** 470-75 (1992).
28. W. O. Soboyejo, C. Mercer, J. Schymanski, and S. R. van der Laan, "Investigation of Thermal Shock in a High-Temperature Refractory Ceramics: A Fracture Mechanics Approach," *J. Am. Ceram. Soc.*, **83** [6] 1309-14 (2001).
29. V. R. Vedula, D. J. Green, J. R. Hellmann, and A. E. Segall, "Test Methodology for the Thermal Shock Characterization of Ceramics," *J. Mat. Sci.,* **33** 5427-32 (1998).
30. A. G. Tomba and A. L. Cavalieri, "Evaluation of the Heat Transfer Coefficient in Thermal Shock of Alumina Disks," *Mater. Sci. and Eng.*, **A276** 76-82 (2000).
31. S. Kitaoka, Y. Matsudaira, C-H Chen, and H. Awaji, "Thermal Cyclic Fatigue Behavior of Porous Ceramics for Gas Cleaning," *J. Am. Ceram. Soc.*, **87** 906-13 (2004).
32. F. Hugot and J. C. Glandus, "Thermal Shock of Alumina by Compressed Air Cooling," *J. Eur. Ceram. Soc.*, **27** 1919-25 (2007).
33. M. I. Nieto, R. Martínez, L. Mazerolles, and C. Baudín, "Improvement in the Thermal Shock Resistance of Alumina Through the Addition of Submicron-sized Aluminum Nitride Particles," *J. Eur. Ceram. Soc.*, **24** 2293-01 (2004).
34. M. Ishitsuka, T. Sato, T. Endo, and M. Shimada, "Thermal Shock Fracture Behavior of ZrO_2 Based Ceramics," *J. Mater. Sci. Lett.*, **24** 4057-61 (1989).
35. K. J. Konsztowicz, "Crack Growth and Acoustic Emission in Ceramics During Thermal Shock," *J. Am. Ceram. Soc.*, **73** [3] 502-08 (1990).
36. S. Mezquita, R. Uribe, R. Moreno, and C. Baudín, "Influence of Mullite Additions on Thermal Shock Resistance of Dense Alumina Materials, Part 2: Thermal Properties and Thermal Shock Behavior," *Brit. Ceram. Trans.*, **100** 246-50 (2001).
37. K. Tagashira, T. Mikami, J. Okamura, T. Sasa, and M. Obata, "Thermal Shock Test of Ceramics by Helium Gas Cooling through a Narrow Slit," *JSME Int. J., Series A*, **45** [4] 612-19 (2002).
38. K. Niihara, J. P. Singh, and D. P. H. Hasselman, "Observations on the Characteristics of a Fluidized Bed for the Thermal Shock Testing of Brittle Ceramics," *J. Mater. Sci.*, **17** 2553-59 (1982).
39. J. Absi and J. C. Glandus, "Improved Method for Severe

Thermal Shocks Testing of Ceramics by Water Quenching," *J. Eur. Ceram. Soc.*, **24** 2835-38 (2004).
40. F. Osterstock, I. Monot, G. Desgardin, and B. L. Mordike, "Influence of Grain Size on the Toughness and Thermal Shock Resistance of Polycystalline," *J. Eur. Ceram. Soc.*, **16** 687-94 (1996).
41. M. Enoki and T. Kishi, "Evaluation of Stochastic Microfracture Process of Particle Dispersed Composites," *Mater. Trans., JIM,* **37** [3] 399-03 (1996).
42. H. Tanaka, S. Honda, T. Nishikawa, and H. Awaji, "Thermal Shock Test for Ceramics by a Water-Flow Cooling Method," *J. Ceram. Soc. Jpn, Supplement* ,**112** [5] S299-04 (2004).
43. P. F. Becher, "Effect of Water Bath Temperature on the Thermal Shock of Al_2O_3," *J. Am. Ceram. Soc.*, **64** C17-C18 (1981).
44. A. F. Emery and A. S. Kobayashi, "Transient Stress Intensity Factors for Edge and Corner Cracks in Quench-Test Specimens," *J. Am. Ceram. Soc.*, **63** 410-415 (1980).
45. S. Honda, S. Hayakawa, T. Nishikawa, and H. Awaji, "Water-Quench Thermal Shock Testing for Ceramic Disks," *J. Ceram. Soc. Jpn*, **108** [2] 166-71 (2000).
46. H. Tanaka, Y. Maki, K. Tsuboi, S. Honda, T. Nishikawa, and H. Awaji, "Thermal Stresses in Porous Materials under Thermal Shock by Cooling Medium – Infiltration Effect on Thermal Stress Distributions -," *J. Ceram. Soc. Jpn.*, **112** 172-78 (2004).
47. D. P. H. Hasselman, E. P. Chen, and P. A. Urick, "Prediction of the Thermal Fatigue Resistance of Indented Glass Rods," *Am. Ceram. Soc. Bull.*, **57** 190-92 (1978).
48. F. Osterstock, "Contact Damage Submitted to Thermal Shock: a Method to Evaluate and Simulate Thermal Shock Resistance of Brittle Materials," *Mater. Sci. and Enging.*, **A168** 41-44 (1993).
49. S. R. Choi and J. A. Salem, "Thermal Shock Behavior of Silicon Nitride Flexure Beam Specimens with Indentation Cracks," *J. Am. Ceram. Soc.*, **77** [3] 833-38 (1994).
50. T. Andersson and D. J. Rowcliffe, "Indentation Thermal Shock Test for Ceramics," *J. Am. Ceram. Soc.*, **79** [6] 1509-14 (1996).
51. S-K. Lee, J. D. Moretti, M. J. Readey, and B. R. Lawn, "Thermal Shock Resistance of Silicon Nitrides Using an Indentation-Quench Test," *J. Am. Ceram. Soc.*, **85** [1] 279-81 (2002).
52. P. Pettersson, M. Johnsson and Z. Shen, "Parameters for Measuring the Thermal Shock of Ceramic Materials with an Indentation-Quench Method," *J. Eur. Ceram. Soc.*, **22** 1883-89 (2002).
53. R. Uribe and C. Baudín, "Influence of a Dispersion of Aluminum Titanate Particles of Controlled Size on the Thermal Shock Resistance of Alumina," *Am. Ceram. Soc.*, **86** 846-50 (2003).
54. A. Kovalčíková, J. Dusza, and P. Šajgalík, "Thermal Shock Resistance and Fracture Toughness of Liquid-Phase-Sintered SiC-based Ceramics," *J. Eur. Ceram. Soc.*, **29** 2387-94 (2009).
55. G. D. Quinn and R. C. Bradt, "On the Vickers Indentation Fracture Toughness Test," *J. Am. Ceram. Soc.*, **90** 673-80 (2007).
56. M. Nawa, K. Yamazaki, T. Sekino, and K. Niihara, "Microstructure and Mechanical Behavior of 3Y-TZP/Mo Nanocomposites Possessing a Novel Interpenetrated Intragranular Microstructure," *J. Mater. Sci.*, **31** 2849-58 (1996).
57. S. Sato, K. Sato, Y. Imamura, and J. Kon, "Determination of the Thermal Shock Resistance of Graphite by Arc Discharge Heating," *Carbon*, **13** 309-16 (1975).
58. S. Sato, H. Awaji, and H. Akuzawa, "Evaluation of the Thermal Shock Fracture Toughness of Reactor Graphites by Arc Discharge Heating," *Carbon*, **16** 103-09 (1978).
59. C. Schubert, H. A. Bahr, and H. J. Weiss, "Crack Propagation and Thermal Shock Damage in Graphite Disks Heated by Moving Electron Beam," *Carbon*, **24** [1] 21-28 (1986).
60. R. Benz, A. Naoumidis, and H. Nickel, "Thermal Shock Testing of Ceramics with Pulsed Laser Irradiation," *J. Nucl. Mater.*, **150** 128-39 (1987).
61. S. Akiyama, S. Amada, M. Shimada, and T. Yoshii, "Estimation of Thermal Shock Resistance of Al_2O_3 Ceramics by Laser Irradiation," *JSME Int. J., Ser. A*, **38** [4] 594-600 (1995).
62. S. Amada, W. Y. Nong, Q. Z. Min, and S. Akiyama, "Thermal Shock Resistance of Carbon-Carbon (C/C) Composites by Laser Irradiation Technique,"*Ceram. Int.*, **25** 61-67 (1999).
63. J-H. Kim, Y-S. Lee, D-H. Kim, N-S. Park, J. Suh, J-O. Kim, and S-I. Moon, "Evaluation of Thermal Shock Strength for Graphite Materials Using a Laser Irradiation Method," *Mater. Sci. & Eng.*, **A 387-389** 385-89 (2004).
64. G. C. Wei and J. Walsh, "Hot-Gas-Jet Method and Apparatus for Thermal-Shock Testing," *J. Am. Ceram. Soc.*, **72** [7] 1286-89 (1989).
65. J. Lamon and D. Pherson, "Thermal Stress Failure of Ceramics under Repeated Rapid Heatings," *J. Am. Ceram. Soc.*, **74** [6] 1188-96 (1991).
66. G. A. Schneider and G. Petzow, "Thermal Shock Testing of Ceramics – A New Testing Method," *J. Am. Ceram. Soc.*, **74** [1] 98-02 (1991).
67. H. Awaji and T. Endo, "Thermal Shock Fracture Testing for Float Glass by Infrared Radiation Technique (*in Jpn*)," *J. Ceram. Soc. Jpn*, **103** [9] 960-65 (1995).
68. H. Awaji, S. Honda, and T. Nishikawa, "Thermal Shock Parameters of Ceramics Evaluated by Infrared Radiation Heating," *JSME Int. J., Series A*, **40** [4] 414-22 (1997).
69. T. Endo, Japanese Utility Model Registration Application No. 59-79600, March 31, 1984.
70. T. Endo, Japanese Patent Application No. 60-50437, March 15, 1985.
71. S.S. Manson, "Behavior of Materials Under Conditions of Thermal Stress," *NACA TN* **2933** 317-50 (1953).
72. R. L. Coble and W. D. Kingery, "Effect of Porosity on Thermal Stress Fracture," *J. Am. Ceram. Soc.*, **38** 33-37 (1955).
73. Y. W. May and A. G. Atkins, "Fracture Toughness and Thermal Shock of Tool and Turbine Ceramics," *J. Mater. Sci.*, **10** 1904-19 (1973).
74. D. Lewis, "Comparison of Critical ΔT_c Values in Thermal Shock with the R Parameter," *J. Am. Ceram. Soc.*, **63**

713-714 (1980).
75. K. Anzai and H. Hashimoto, "Thermal Shock Resistance of Silicon Nitride," *J. Mater. Sci.*, **12** 2351-53 (1997).
76. S. P. Timoshenko and J. N. Goodier, "Theory of Elasticity", pp.433-84, McGraw-Hill Book Co., New York, 1934.
77. S. Honda, T. Takahashi, S. Morooka, S. Zhang, T. Nishikawa, and H. Awaji, "Thermal Stress and Stress Intensity Factor Considering Temperature Dependent Material Properties (*in Jpn*)," *J. Soc. Mater. Sci. Jpn*, **46** 1300-05 (1997) .
78. H. Awaji, H-J. Xian, H. Tanaka, and S. Honda, "Water-Flow Cooling and Infrared Radiation Heating Techniques for Thermal Shock Test of Ceramics," pp. 557-60, Proc. sixth international congress on thermal stresses, May 26-29, Vienna, 2005.
79. W. P. Rogers, A. F. Emery, R. C. Bradt, and A. S. Kobayashi, "Statistical Study of Thermal Fracture of Ceramic Materials in the Water Quench Test," *J. Am. Ceram. Soc.*, **70** [6] 406-12 (1987).
80. T. Sakuma, U. Iwata, and H. Takaku, "Estimation of Thermal Shock Resistance of Ceramics (4^{th} Report) (*in Jpn*)," *Trans. JSME*, **58A** 1424-29 (1992).
81. W-J. Lee, Y. Kim, and E. D. Case, "The Effect of Quenching Media on the Heat Transfer Coefficient of Polycrystalline Alumina," *J. Mater. Sci.*, **28** 2079-83 (1993).
82. T. Nishikawa, T, Gao, M. Hibi, and M. Takatsu, "Heat Transmission during Thermal Shock Testing of Ceramics," *J. Mater., Sci.*, **29** 213-17 (1994).
83. R. Badaliance, D. A. Krohn, and D. P. H. Hasselman,"Effect of Slow Crack Growth on the Thermal-Stress Resistance of an Na_2O-CaO-SiO_2 Glass," *J. Am. Ceram. Soc.*, **57** 432-36 (1974).
84. H. Awaji, S. Honda, and T. Nishikawa, "Statistical Approach to Strength Degradation Analysis during Water Quenching," *J. Ceram. Soc. Jpn*, **106** [6] 551-54 (1998).
85. M. Oguma and T. Motomiya, "A BET Surface Area Measurement Technique for Evaluation of Crack Extension in Alumina Pellets Subjected to Thermal Shock," *J. Ceram. Soc. Jpn*, **97** 778-82 (1989).
86. M. Hefetz and S. I. Rokhlin, "Thermal Shock Damage Assessment in Ceramics Using Ultrasonic Waves," *J. Am. Ceram. Soc.*, **75** [7] 1839-45 (1992).
87. D. N. Boccaccini, M. Romagnoli, P. Veronesi, M. Cannio, C. Leonelli, G. Pellacani, T. V. Husovic, and A. R. Boccaccini, "Quality Control and Thermal Shock Damage Characterization of High-Temperature Ceramics by Ultrasonic Pulse Velocity Testing," *Int. J. Appl. Ceram.Technol.*, **4** [3] 260-68 (2007).
88. W. J. Lee and E. D. Case, "Thermal Fatigue in Polycrystalline Alumina," *J. Mater. Sci.*, **25** 5043-54 (1990).
89. F. Mignard, C. Olagnon, and G. Fantozzi, "Acoustic Emission Monitoring of Damage Evaluation in Ceramics Submitted to Thermal Shock," *J. Eur. Ceram. Soc.*, **15** 651-53 (1995).
90. F. Mignard, C. Olagnon, M. Saadaoui, and G. Fantozzi, "Thermal Shock Behavior of a Coarse Grain Porous Alumina," *J. Mater. Sci.*, **31** 2437-41 (1996).
91. L. J. Vandeperre, A. Kristfferson, E. Carlsröm, and W. J. Clegg, "Thermal Shock of Layered Ceramic Structures with Crack-Deflecting Interfaces," *J. Am. Ceram. Soc.*, **84** 104-10 (2001).
92. D. Sherman, "Alumina/NiCu Laminate under Thermal Shock up to 1000C: I, Experimental," *J. Am. Ceram. Soc.*, **84** 2819-26 (2001).
93. K. Kokini, J. DeJonge, S. Rangaraj, and B. Beardsley, "Thermal Shock of Functionally Graded Thermal Barrier Coatings with Similar Thermal Resistance," *Surface & Coatings Tech.*, **154** 223-31 (2002).
94. A. Kawasaki and R. Watanabe, "Thermal Fracture Behavior of Metal/Ceramic Functionally Graded Materials," *Eng. Fract. Mech.*, **69** 1713-28 (2002).
95. B-L. Wang, Y-W. Mai, and X-H. Zhang, "Thermal Shock Resistance of Functionally Graded Materials," *Acta Mater.*, **52** 4961-72 (2004).
96. G. Jin, M. Takeuchi, S. Honda, T. Nishikawa, and H. Awaji, "Thermal Shock Testing on Mullite/Mo FGM Disks Using an Infrared Radiation/Water Flow Technique," *J. Ceram. Soc. Jpn*, *Supplement,* **112** S286-S290 (2004).
97. G. Jin, M. Takeuchi, S. Honda, T. Nishikawa, and H. Awaji, "Properties of Multilayered Mullite/Mo Functionally Graded Materials Fabricated by Powder Metallurgy Processing," *Mater. Chem. & Phys.*, **89** 238-43 (2005).
98. V. R. Vedula, S. J. Glass, D. M. Saylor, G. S. Rohrer, W. C. Carter, S. A. Langer, and E. R. Fuller Jr., "Residual-Stress Predictions in Polycrystalline Alumina," *J. Am. Ceram. Soc.*, **8**4 2947-54 (2001).
99. T. K. Gupta, "Strength Degradation and Crack Propagation in Thermally Shocked Al_2O_3," *J. Am. Ceram. Soc.*, **55** [5] 249-53 (1972).
100. A. G. Evans, "Microfracture from Thermal Expansion Anisotropy – I. Single Phase Systems," *Acta Metallurgica*, **26** 1845-53 (1978).
101. A. Zimmermann, E. R. Fuller Jr., and J. Rödel, "Residual Stress Distributions in Ceramics," *J. Am. Ceram. Soc.*, **82** 3155-60 (1999).
102. H. Awaji, T. Matsunaga, and S-M. Choi, "Relation between Strength, Fracture Toughness, and Critical Frontal Process Zone Size in Ceramics," *Mater. Trans.*, **47** [6] 1532-39 (2006).
103. K. Niihara, "New Design Concept of Structural Ceramics – Ceramic Nanocomposites-," *J. Ceram. Soc. Jpn*, **99** 974-82 (1991).
104. H. Awaji, "Ceramic-Based Nanocomposites," "Handbook of Nanoceramics and their based Nanodevices, Vol. 2", pp. 231-251, Ed. by T-Y. Tseng and H. S. Nalwa, Am. Sci. Pub, Los Angeles, 2009.
105. H. Okamura, "*Senkei Hakairikigaku Nyuumon* (Introduction to Linear Fracture Mechanics) (*in Jpn*)", p.76 , Baifukan, Tokyo, 1976.
106. S-M. Choi and H. Awaji, "Nanocomposites – a New Material Design Concept," *Sci. & Tech. Advanced Mater.*, **6** 2-10 (2005).